The 2010 IEEE/RSJ International Conference on
Intelligent Robots and Systems
October 18-22, 2010, Taipei, Taiwan

Natural Motion: Efficient Path Tracking With Robotic Limbs

Dragomir N. Nenchev*, Yoichi Handa† and Daisuke Sato*

Abstract— **We aim at experimental verification of the efficiency of natural-motion path tracking (i.e. tracking speed in proportion to the determinant of the Jacobian) in comparison to constant-speed path tracking. This is done first via simulations, with a simple planar manipulator and then with a six-DOF manipulator. From the results it becomes apparent that natural-motion path tracking outperforms constant-speed path tracking in terms of peak joint speed, peak joint torque and total mechanical power, ensuring thereby a higher average tracking speed. The results are also confirmed via experiments with a real six-DOF robotic limb.**

I. Introduction

There are robotic application tasks where exact path tracking of a given workspace path is of primary importance, while the tracking speed along the path can be preset freely. This freedom has been exploited in past studies to meet mainly two objectives: minimum-time path tracking [2]–[4] and keeping control efforts within prescribed limits [5]–[7]. Hollerbach [5], for instance, introduced the concept of *time-scaling* to handle control torque constraints within a dynamic framework. Also, the objectives can be combined in a single optimization framework [8]. Another example is the work of Sampei and Furuta who have shown how time-scaling may help in linearization problems [9], and have applied the idea to ensure stability of motion around kinematic singularities [10]. Generally speaking, the additional DOF gained via relaxing a strict time constraint along the path can be used to decrease control efforts [11]. This, in turn, will enable the controller to deal with uncertainties and lead to robust performance. The method has also been referred to as *path-following* and has been exploited not only in the field of robotic control, but also in that of vehicle control, e.g., flight control [12] and autonomous marine craft control [13].

In our previous work [1], [14] we have shown that when the path tracking speed is set to be in proportion to the determinant of the Jacobian, there is an important impact on the motion dynamics: the dynamic system is transformed into an autonomous system, and in addition, the control torque can be derived from a pure (configuration-dependent) potential function. We called this type of motion "natural motion," in harmony with both the kinematic constraint, deduced from the "natural parameter" of a certain curve in augmented configuration space, and the dynamic properties of energy-conserving "natural systems" [15].

The authors are with the Department of Mechanical Systems Engineering, Faculty of Engineering, Tokyo City University, Tamazutsumi 1-28-1, Setagaya-ku, Tokyo 158-8557, Japan.
* {nenchev,dsato}@tcu.ac.jp
† {handa}@rls.mse.tcu.ac.jp

So far, path tracking under natural motion has not been studied in detail. The aim of this work is to examine experimentally the performance of natural motion path tracking with a nonredundant robotic limb. Our goal is to expose quantitatively the advantages of natural motion when compared to a constant-speed path tracking task with the same limb.

II. Background and Notation

Consider a robot limb with n joint variables $\boldsymbol{q} = (q_1, q_2, ..., q_n)$ and m end-link position/orientation variables $\boldsymbol{x} = (x_1, x_2, ..., x_m)$. The velocity relation is given by:

$$\boldsymbol{\nu} = \boldsymbol{J}(\boldsymbol{q})\dot{\boldsymbol{q}}, \tag{1}$$

where $\boldsymbol{\nu} \in \Re^m$ denotes the coordinates of the *end-link twist* and $\boldsymbol{J}(\boldsymbol{q})$ is the limb Jacobian. Here and henceforth, we will assume that all joint variables represent angles. The configuration space $\mathcal{C}$, a subspace of $\Re^n$, will be then uniform in terms of physical units[1]. Euclidean vector norm $\|\circ\|$ can be employed then. The last equation solves the direct kinematics problem for the velocities.

A. Singularity-Consistent Inversion

The *inverse kinematics* problem plays an important role in path planning and tracking control. We will make use here of the singularity-consistent solution method because of its inherent stability property in the vicinity of singularities. The notation is briefly reviewed below, for further details interested readers are referred to [16].

First, we assume the end-link moves along a smooth parameterized path $\boldsymbol{x}(q_*)$, q_* denoting the path parameter. The end-link twist, at a given point q_*, can be represented as

$$\boldsymbol{\nu}(q_*, \dot{q}_*) = \boldsymbol{t}_*(q_*)\dot{q}_* \tag{2}$$

where $\boldsymbol{t}_*(q_*)$ is the normalized end-link twist, obtained when the speed of the parameter is $\dot{q}_* = 1$ rad/s. Further on, it is convenient to augment the configuration space with the path parameter q_*. We then obtain the *augmented configuration space* $\mathcal{C}^*$, a subspace of $\Re^{n+1}$, with elements $\bar{\boldsymbol{q}} \equiv (\boldsymbol{q}, q_*)$. With this notation, (1) can be represented in homogeneous form as:

$$\overline{\boldsymbol{J}}(\bar{\boldsymbol{q}})\dot{\bar{\boldsymbol{q}}} = \boldsymbol{0}, \tag{3}$$

where

$$\overline{\boldsymbol{J}}(\bar{\boldsymbol{q}}) \equiv \begin{bmatrix} \boldsymbol{J}(\boldsymbol{q}) & -\boldsymbol{t}_*(q_*) \end{bmatrix}$$

[1] In case of a mixed-joint structure (with rotational and translation joints), uniformity can be ensured with proper scaling.

is called *the column-augmented Jacobian*.

Besides being homogeneous, (3) is underdetermined and hence, the number of solutions is infinite. Therefore, all solutions must be in the kernel of matrix $\overline{\boldsymbol{J}}$. Let us assume now that the limb is *nonredundant*: $m = n$. For a full-rank column-augmented Jacobian, the kernel contains a single nonzero element then. The set of solutions of (3) is:

$$\dot{\bar{\boldsymbol{q}}} = b\bar{\boldsymbol{n}}(\bar{\boldsymbol{q}}), \tag{4}$$

where b is an arbitrary scalar, and $\bar{\boldsymbol{n}}(\bar{\boldsymbol{q}}) \in \ker\overline{\boldsymbol{J}}(\bar{\boldsymbol{q}}) \subset \Re^{n+1}$. A vector from the kernel can be derived in analytical form with the help of the cofactors of matrix $\overline{\boldsymbol{J}}$ [17]:

$$\bar{\boldsymbol{n}}(\bar{\boldsymbol{q}}) = \begin{bmatrix} C_1 & C_2 & \dots & C_{n+1} \end{bmatrix}^T \tag{5}$$

where $C_i = (-1)^{i+1}\det\overline{\boldsymbol{J}}_i$ is the i-th cofactor, and $\overline{\boldsymbol{J}}_i$ is obtained from matrix $\overline{\boldsymbol{J}}$ by removing the i-th column. The last expression can be rewritten as:

$$\bar{\boldsymbol{n}}(\bar{\boldsymbol{q}}) \equiv \begin{bmatrix} \boldsymbol{n}^T(\bar{\boldsymbol{q}}) & \det\boldsymbol{J}(\boldsymbol{q}) \end{bmatrix}^T \tag{6}$$

where $\boldsymbol{n}(\bar{\boldsymbol{q}}) \equiv [\mathrm{adj}\boldsymbol{J}(\boldsymbol{q})]\,\boldsymbol{t}_*(q_*)$, adj$(\circ)$ denotes the adjoint matrix [18]. Note that $\boldsymbol{n}(\bar{\boldsymbol{q}})$ maps vectors from the augmented configuration space to the tangent space of $\mathcal{C}$ at $\boldsymbol{q}$: $\{\boldsymbol{n}(\bar{\boldsymbol{q}}) : \mathcal{C}^* \subset \Re^{n+1} \rightarrow T\mathcal{C}_q \subset \Re^n\}$.

Equation (4) can be split into two parts to obtain the joint motion differential

$$\dot{\boldsymbol{q}} = b\,\boldsymbol{n}(\bar{\boldsymbol{q}}) \tag{7}$$

and the path parameter differential

$$\dot{q}_* = b\det\boldsymbol{J}(\boldsymbol{q}). \tag{8}$$

Usually, path parameter q_* is considered an independent variable. Then, one determines the scalar b from (8), and substitutes it back into (7) to obtain the joint velocity. Note, however, that in the vicinity of kinematic singularities this may lead to instability since the determinant of the Jacobian is close to zero. The above formulation can alleviate this problem by taking b as the independent parameter. Ultimately, this leads to the inherent stability of the method as will be seen herein (see also [16]).

Finally, it might be worth noting that the physical meaning of parameter b can be understood as a dimensional map adjusting the dimension of the null vector $\bar{\boldsymbol{n}}(\bar{\boldsymbol{q}})$ (volume element in $\Re^n$) to the dimension of joint speed ([rad/s] for rotational joints).

B. The Natural Motion of a Robotic Limb

The trivial reparameterization, b being a nonzero *constant*, plays an important role throughout this work. Note that when $\underline{b}$ is constant (constant quantities will be underlined henceforth), (4) can be regarded as an autonomous dynamic system. The flow of vector field $\bar{\boldsymbol{n}}(\bar{\boldsymbol{q}})$ is represented then by a set of spatial curves in augmented configuration space $\mathcal{C}^*$. Motion along a specific curve (determined from the initial condition) can be associated with the so called *self motion* of a kinematically redundant limb obtained from the original limb by adding a virtual joint with q_* as the joint variable. The curve will be referred to as the *self-motion manifold* [19]. We will restrict our analysis to self-motion manifolds made of regular points of the autonomous dynamic system[2]. The self-motion manifold can then be characterized by the invariant arc length λ, also called natural parameter. λ is determined uniquely up to an additive constant, from $\dot{\lambda} = \|\bar{\boldsymbol{n}}\|$. It should be apparent then that under natural motion the magnitude of the end-link twist and hence, the path tracking speed, will be in proportion to $|\det\boldsymbol{J}|$.

C. Natural Motion Dynamics

The conventional form of the equation of motion is:

$$\boldsymbol{M}(\boldsymbol{q})\ddot{\boldsymbol{q}} + \boldsymbol{C}(\boldsymbol{q},\dot{\boldsymbol{q}})\dot{\boldsymbol{q}} + \boldsymbol{g}(\boldsymbol{q}) = \boldsymbol{\tau}, \tag{9}$$

where $\boldsymbol{M}(\boldsymbol{q})$ is the symmetric positive-definite limb inertia matrix, $\boldsymbol{C}(\boldsymbol{q},\dot{\boldsymbol{q}})\dot{\boldsymbol{q}}$ and $\boldsymbol{g}(\boldsymbol{q})$ denote Coriolis and centrifugal, and gravity forces, respectively, $\boldsymbol{\tau}$ stands for the driving joint torque. Making use of the joint velocity representation (7) and the respective time differential, the equation of motion can be rewritten as:

$$\Big(\dot{b}\boldsymbol{M}(\boldsymbol{q}) + b\boldsymbol{A}(\bar{\boldsymbol{q}})\Big)\,\boldsymbol{n}(\bar{\boldsymbol{q}}) + \boldsymbol{g}(\boldsymbol{q}) = \boldsymbol{\tau}, \tag{10}$$

where

$$\boldsymbol{A}(\bar{\boldsymbol{q}}) \equiv b\boldsymbol{M}(\boldsymbol{q})\frac{\partial\boldsymbol{n}(\bar{\boldsymbol{q}})}{\partial\bar{\boldsymbol{q}}} + \boldsymbol{C}(\boldsymbol{q},\dot{\boldsymbol{q}}).$$

We are referring to (10) as the *singularity-consistent parameterization of the equation of motion* [1], [14].

Next, note that under natural motion, the force component $\dot{b}\boldsymbol{M}(\boldsymbol{q})\boldsymbol{n}(\bar{\boldsymbol{q}})$ in the direction of generalized momentum is zero since b is constant. Then, (10) becomes:

$$\underline{b}\boldsymbol{A}(\bar{\boldsymbol{q}})\boldsymbol{n}(\bar{\boldsymbol{q}}) + \boldsymbol{g}(\boldsymbol{q}) = \boldsymbol{\tau}. \tag{11}$$

It is easy to show that this is a pure potential system. Natural motion can be also characterized as nondissipative motion along the prespecified path, with initial energy derived from the specified constant $\underline{b}$. Note also that the energy is quadratic in $\underline{b}$, while the instantaneous mechanical power is cubic.

III. Natural Motion Path Tracking: A Comparative Analysis

Tracking performance under natural motion along a specified path in the workspace will be examined below and compared with results from constant-speed tracking along the same path.

A. Simple Example

First, we consider a simple planar 2R limb tracking a circle with its end-tip. The current point on the circle is determined by the path parameter angle q_*, (x_c, y_c) denote the circle center coordinates, r is its radius (see Fig. 1). For this simple example all quantities can be derived in analytical form (see [1], p. 19). Each link is modeled as a thin rod of one meter length, having a mass of 1 kg, with respective link inertia and center of mass located in the middle. The initial limb

[2]The regular points of the autonomous system are the points where the linear system (1) is nonsingular or where it is singular with codimension one (an inconsistent system) [1].

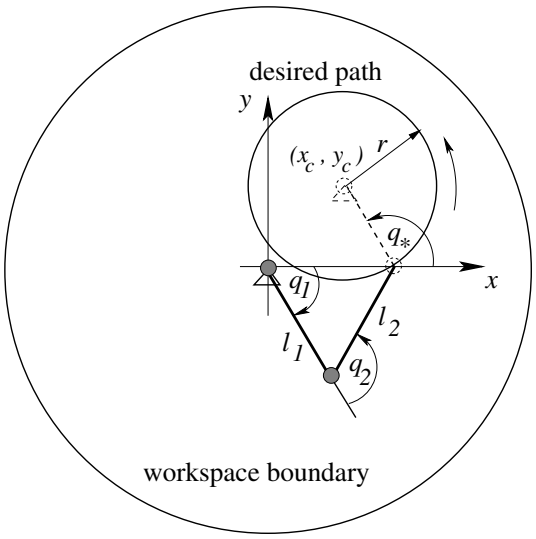

Fig. 1. Simple 2R limb tracking a circular path.

TABLE I

PATH-TRACKING CASES WITH THE 2R LIMB (NOMINAL MODEL).

case	CS-1	NM-1	NM-2	NM-3	CS-2
distance traveled [m]	8.85	8.85	30.43	24.75	24.75
peak joint speed [rad/s]	2.9	0.84	2.9	2.26	7.73
peak joint torque [Nm]	5.31	0.73	8.74	5.31	37.8
total mechanical power [W]	626.7	149.15	5,751.0	2,747.4	11,167.3

NM: natural motion CS: constant-speed

configuration is set to -60 and 120 deg. The desired path radius is 0.7 m, while the center of the circle is determined via the initial $q_* = 120$ deg. The initial configuration as well as the location of the circle within the workspace are those shown in Fig. 1. It should be apparent that the circle passes through the vicinity of a kinematic singulary near the workspace outer boundary.

The desired path is tracked for two full cycles, with the well known resolved acceleration dynamic feedback controller. The natural motion tracking speed is set via the constant $\underline{b} = 1.2$ rad/s m^{-2}. Constant-speed tracking is achieved, on the other hand, through the constant $\dot{q}_* = 0.85$ rad/s. These two values have been choosen so that the same distance (two full cycles) is tracked for the same time.

In the first set of simulations, we assume the model is perfect and no external disturbances are present. This assumption is not realistic, but initially it helps for better understanding the difference in path tracking performance. The results from natural-motion path tracking are shown on the left side of Fig. 2, and those from constant-speed tacking on the right side. They include graphs for the joint angles, the joint speeds including the path parameter speed $\dot{q}_*$, the end-tip speeds, the determinant and the joint torque. The first feature clearly seen is the significant difference in peak joint speed and peak joint torque: 2.9 rad/s and 5.31 Nm, respectively, for constant-speed tracking versus 0.84 rad/s and 0.73 Nm for natural motion. This is over three times higher peak speed and over seven times larger joint torque requirement for constant-speed tracking. These peak values are due to the singularity, as can be inferred from the determinant graphs. In addition, we calculated the total mechanical power for each run. The results, given in Table I (cases CS-1 and NM-1 respectively), show that natural motion can be performed with one quater or less of the total power requirement of constant-speed tracking along the same path for the same distance and time.

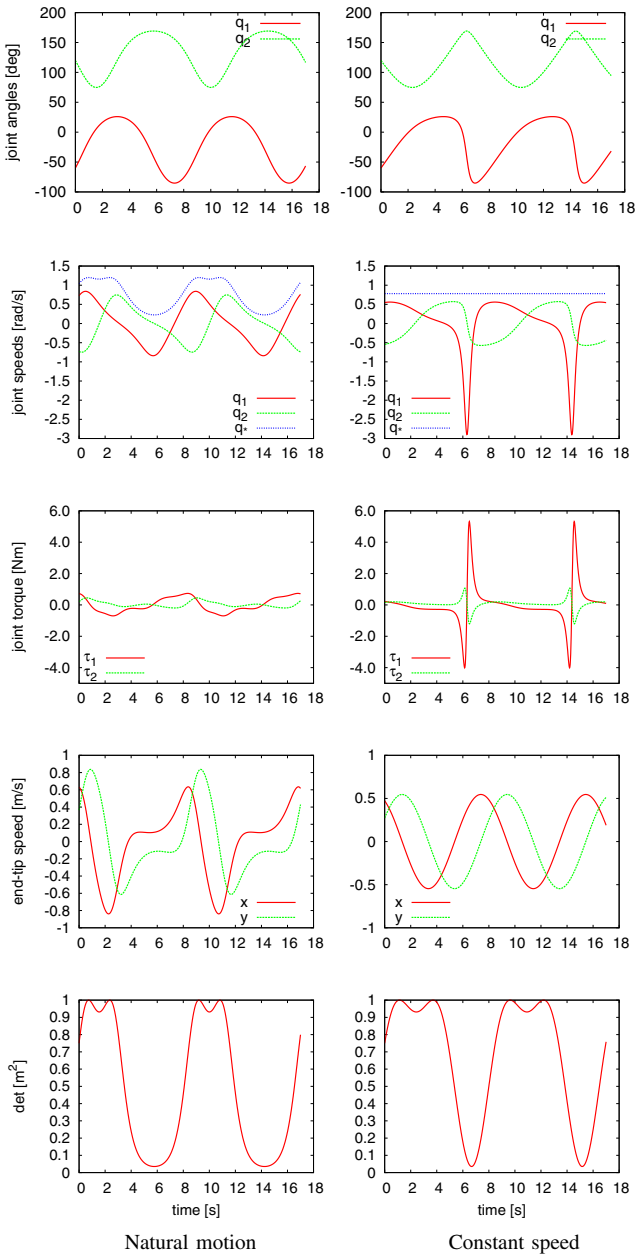

Fig. 2. 2R path tracking with perfect model and no external disturbance.

Another notable feature of natural motion is the smoothness of the joint space curves when compared to those of constant-speed tracking. Indeed, from Fig. 2 it is clearly seen that in the case of constant-speed tracking, both the

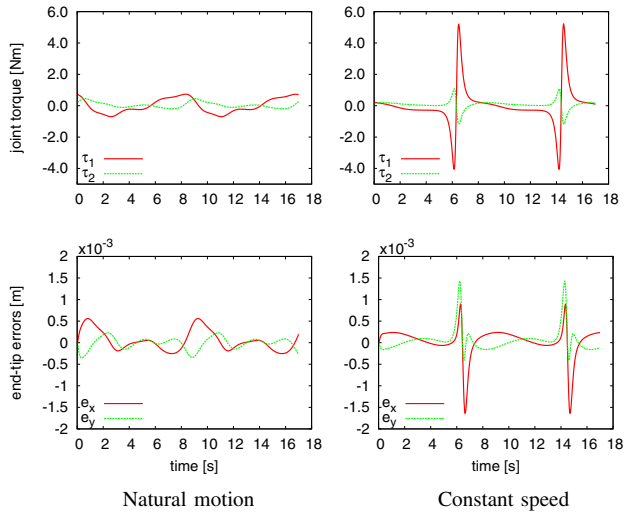

Fig. 3. 2R path tracking with imperfect model.

joint velocity and the joint torque increase rapidly when approaching the singularity. On the other hand, the respective curves for natural motion are quite smooth. This can be explained with the fact that the curvature of the self-motion manifold increases rapidly in the neighborhood of the singularity, which also influences the motion dynamics. Constant-speed tracking does not account for the changes in curvature, hence the large fluctuations. In workspace, on the other hand, the end-tip speed is uniform for constant-speed tracking, while under natural motion the end-tip speed fluctuates a bit more, decelerating when approaching the singularity neighborhood, and accelerating when departing from it. The fluctuations are not as large, though, as in joint space.

Two more simulations were performed under natural motion, one with the peak joint speed and the other with the peak joint torque obtained during the previous simulation. From Table I (case NM-2) it is seen that with the same peak joint velocity as constant-speed motion, under natural motion the end-tip could travel more than three times farther. Since we didn't change the tracking time (17 s), this clearly shows that a much higher *average speed* can be achieved under natural motion. A similar result was obtained when the same peak joint torque was used while tracking (case NM-3). Again, natural motion outperformed constant-speed tracking in terms of distance traveled, and hence, average speed. We confirmed once again the ratio between the peak values and the power obtained earlier, by tracking the path for the same distance as in case NM-3, with constant-speed (see Table I, case CS-2).

In the next set of simulations, path tracking in the presence of modeling errors was examined. In the resolved acceleration controller, the masses and moments of inertia of the links were modified to have 10% deviation from the nominal values. The same desired path and same initial conditions as in the previous simulation set were assigned. The results in terms of joint torque and end-tip path tracking errors are shown in Fig. 3. Note that joint angle, joint speed, end-tip speed and determinant data graphs are same as those shown in Fig. 2. This can be inferred from the small tracking errors. Comparing the torque graphs, one can draw similar conclusions as in the previous case. Both the peak torque values and the torque variations are much larger in the case of constant-speed tracking. The power requirement for constant-speed tracking was also much larger (over four times) than that for natural motion.

It is interesting to note that the path tracking errors behave in a similar way: the maximum error for constant-speed tracking was over 1.5 mm, while for natural motion it was less than 0.6 mm, the error graphs for natural motion being much smoother than those for constant-speed tracking. This can be explained again with the rapidly increasing curvature in the neighborhood of the singularity, which also influences the error dynamics.

B. Six-DOF Example

The next simulation example is a 6R manipulator, the end link tracking a circular path and keeping thereby a constant orientation. The same manipulator will be used later for the experiments. This is a seven-DOF Mitsubishi Heavy Industries PA-10 manipulator (see Fig. 4). Since we have restricted the scope to nonredundant manipulators in this study, the third joint is immobilized during the experiments. The link lengths are 0.45 m, 0.5 m and 0.08 m respectively for the lower arm, upper arm and the wrist. The initial configuration is $\begin{bmatrix}15.0 & -37.0 & 0.0 & 80.0 & 15.0 & -45.0 & -15.0\end{bmatrix}$ deg. The desired circular path is centered at a distance (radius) of $r = 0.2$ m from the initial position along x_a. Further on, a relevant set of kinematic singularities[3] is displayed in the figure as a vertical line along the z_0 axis. The desired path passes by this singularity set, the closest distance being 0.07 m.

The desired path was tracked again for two full cycles. We used an inverse Jacobian kinematics controller as a path tracking controller. The joint torque was calculated from the nominal model with suitably chosen dynamic parameters. We assumed that the gravity torque is fully compensated. The natural motion tracking speed was set via the constant $\underline{b} = 1.361$ rad/s m^{-1}, while that for constant speed tracking — through the constant $\underline{\dot{q}}_* = 0.277$ rad/s. Since we are going to track the same path with the real robot, we had to insert acceleration/deceleration portions along the path. For this purpose we used a fifth order spline in the parameters (b and $\dot{q}_*$) of 2 s at the beginning/end of a 60 s interval for path tracking. The results are shown in Fig. 5. The main conclusion made in the previous simulation with the 2R limb can be reaffirmed. Constant-speed tracking yields larger variations in joint velocity and joint torque than natural motion, which is clearly due to the vicinity of the kinematic singularity, as can be inferred from the determinant graphs. The peak values are given in Table II (cases NM-1 and CS-1). Similar to the 2R example, it can be seen that constant-speed

[3]The set of so-called "shoulder singularities".

tracking requires about three times larger peak joint speed than natural motion, and also about three times larger peak joint torque. The total power requirement was about twice as that for natural motion. From the other cases (NM-2 and NM-3) it is seen that a higher average motion speed can be achieved under natural motion if the peak speed (case NM-2) or the peak torque (case NM-3) is applied, since the distance traveled is larger, for the same tracking time.

Finally, we present experimental data from the real robot in Fig. 6. The velocity data derived from the joint encoders matches well with the simulation data in Fig. 5. The torque data obtained via the electrical current sensors of the controller, on the other hand, are quite different from those in the simulations. The reason is that unmodeled dynamic components such as joint friction, model uncertainty, etc. are prevailing in some of the joints. For instance, from the constant-speed simulation torque graph in Fig. 5, it may be seen that Joint 1 and Joint 2 are driven with peak torque around the singularity. The respective graph in the experiments (Fig. 6) shows that only Joint 1 appears to be experiencing such peak torque. A comparison for the torque requirement in that joint while tracking with natural motion and with constant speed can be made with the help of Fig. 7. The advantage of natural motion can be confirmed in this case (about 40% less peak torque requirement). A video clip is attached to the paper showing the results from this simulation by overlaid movie images for natural motion and constant-speed tracking.

It should be mentioned that although the specific path examined here was a planar curve, the results obtained are valid for any spatial curve since the (Riemannian) structure of the self-motion manifold in augmented configuration space does not depend upon the particular end-effector path. We should note also that the advantages of natural motion are most apparent for paths inducing larger manifold curvatures, i.e. those paths that pass close by singularities. In practice,

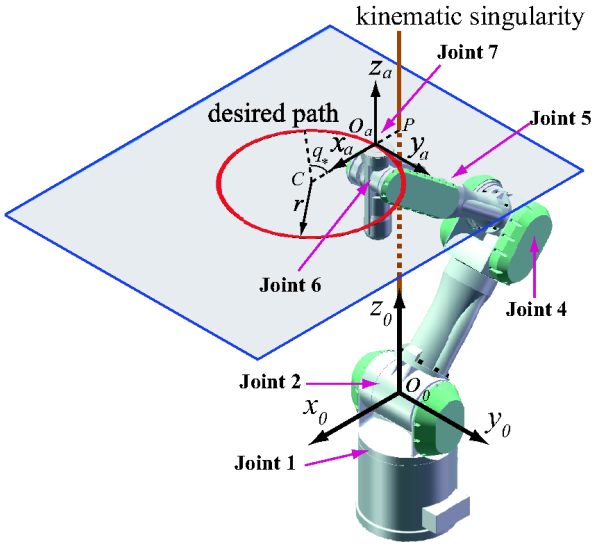

Fig. 4. 6R manipulator tracking a circular path. This is actually a model of a seven-DOF manipulator with one joint locked (Joint 3, not shown).

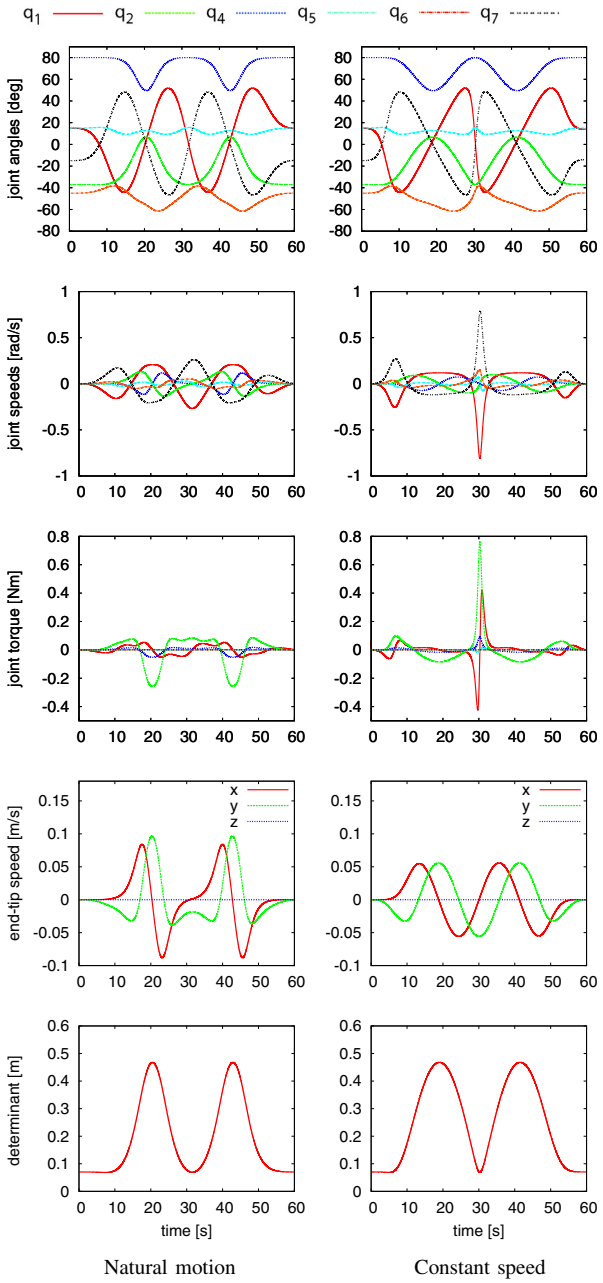

Fig. 5. Path tracking simulation with the 6R manipulator.

such paths shouldn't be considered as special cases; paths passing close by spherical wrist singularities, for example, are quite common.

IV. Conclusions

We examined end-link path tracking with a special speed profile obtained while a robotic limb performs natural motion. The comparative analysis with constant-speed path tracking revealed that natural motion is superior in terms of smoothness of motion in joint space, requiring thereby less peak joint velocity and peak joint torque. This also implies that higher average tracking speeds can be ensured. Moreover, natural motion also significantly outperformed constant-speed tracking in terms of the total mechanical power requirement.

TABLE II

PATH-TRACKING CASES WITH THE 6R MANIPULATOR.

	CS-1	NM-1	NM-2	NM-3
distance traveled [m]	2.51	2.51	7.63	4.18
peak joint speed [rad/s]	0.803	0.268	0.803	0.460
peak joint torque [Nm]	0.750	0.258	2.27	0.750
total mechanical power [W]	486.65	222.78	5939.3	1100.2

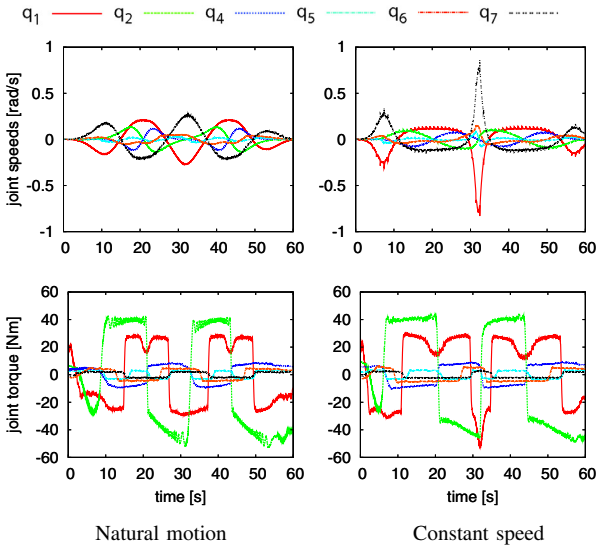

Fig. 6. Path tracking experiment with the 6R manipulator.

It must be noted that natural motion does not directly optimize such quantities as time and/or control efforts. The approach is quite different from the existing methods mentioned in the Introduction, since none of them makes explicit use of the natural metrics and the Riemannian structure of the embedded self-motion manifold. It would be interesting to extend the comparative analysis in this direction. Nevertheless, we believe that the advantages of natural motion highlighted here in comparison to constant-speed path tracking, plus the easy implementation and the capability of motion through singularities, known from a previous work, make natural motion path tracking an appealing motion generation alternative.

Finally, we should mention that inspite of the present focus on nonredundant robotic limbs, it should be possible to extend the results to redundant limbs by expanding the dimension of the self-motion manifold and by involving relevant geometrical concepts.

ACKNOWLEDGMENTS

The help of Mr. Jun Takahashi in deriving the dynamic model of PA-10 is acknowledged.

REFERENCES

[1] D. N. Nenchev, "Natural motion and singularity-consistent inversion of robot manipulators," in *Advances in Robot Control,* Springer Berlin Heidelberg, pp. 9–33, 2007.

[2] K. G. Shin and N. D. McKay, "Minimum-time control of robotic manipulator with geometric path constraints," *IEEE Trans. on Automatic Control*, vol. AC-30, no. 6, pp. 531–541, June, 1985.

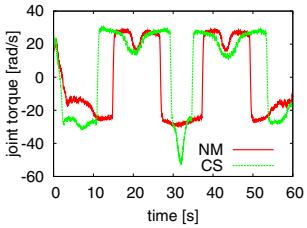

Fig. 7. Joint 1 torque comparison from the experiment.

[3] J. E. Bobrow, S. Dubowski and J. S. Gibson, "Time-optimal control of robotic manipulators along specified paths," *Int. J. of Robotics Research,* vol. 4, no. 3, pp. 3–17, 1985.

[4] F. Pfeiffer and R. Johanni, "A concept for manipulator trajectory planning," *IEEE J. of Robotics and Automation,* vol. RA-3, no. 2, pp. 115–123, 1987.

[5] J. M. Hollerbach, "Dynamic scaling of manipulator trajectories," *Trans. ASME, J. of Dynamic Systems, Measurment and Control,* vol. 106, pp. 102–106, March, 1984.

[6] H. Arai, K. Tanie, and S. Tachi, "Path tracking control of a manipulator considering torque saturation," *IEEE Trans. on Industrial Electronics,* vol. 41, no. 1, pp. 25–31, Feb, 1994.

[7] O. Dahl and L. Nielsen, "Torque-limited path following by on-line trajectory time scaling," *IEEE Trans. Robotics and Automation,* vol. 6, no. 5, pp. 554–561, 1994.

[8] Z. Shiller and S. Dubowsky, "Robot path planning with obstacles, actuator, gripper, and payload constraints," *Int. J. of Robotics Research,* vol. 8, no. 6, pp. 3–18, Dec, 1989.

[9] M. Sampei and K. Furuta, "On time scaling for nonlinear systems: application to linearization," *IEEE Trans. on Automatic Control,* Vol. AC-31, No. 1, pp. 459–462, May, 1985.

[10] M. Sampei and K. Furuta, "Robot control in the neighborhood of singular points," *IEEE J. of Robotics and Automation,* vol. 4, no. 3, pp. 303–309, June 1988.

[11] D. B. Dačić, M. V. Subbotin, and P. V. Kokotović, "Control effort reduction in tracking feedback laws," *IEEE Tran. on Automatic Control,* vol. 51, pp. 1831–1837, November, 2006.

[12] S. A. Al-Hiddabi and N. H. McClamroch, "Tracking and maneuver regulation for nonlinear nonminimum phase systems: application to flight control," *IEEE Trans. Control Syst. Technol.,* vol. 10, no. 6, pp. 780–792, June, 2002.

[13] L. Lapierre, D. Soetanto, and A. Pascoal, "Nonlinear path following with applications to the control of autonomous underwater vehicles," in *Proc. 42nd IEEE Conf. Decision Control,* Maui, USA, 2003, pp. 1256–1261.

[14] D. N. Nenchev and M. Uchiyama, "Natural motion analysis based on the singularity-consistent parameterization," in *Proc. 1997 IEEE Int. Conf. Robotics and Automation,* Albuquerque, USA, 1997, pp. 2683–2688.

[15] V. I. Arnold. "Mathematical methods of classical mechanics," *Springer-Verlag,* New York Inc., 1989.

[16] D. N. Nenchev, Y. Tsumaki, and M. Uchiyama, "Singularity-consistent parameterization of robot motion and control," *Int. J. of Robotics Research,* vol. 19, no. 2, pp. 159–182, 2000.

[17] J. Baillieul, "Kinematic programming alternatives for redundant manipulators," in *Proc. IEEE Int. Conf. Robotics and Automation,* St. Louis, USA, 1985, pp. 722–728.

[18] Y. Tsumaki, D. N. Nenchev, S. Kotera and M. Uchiyama, "Teleoperation based on the adjoint jacobian approach," *IEEE Control Sytems Magazine,* vol. 17, no. 1, pp. 53–62, 1997.

[19] J. Burdick, "A classification of 3R regional manipulator singularities and geometries," in *Proc. IEEE Int. Conf. on Robotics and Automation,* Sacramento, California, 1991, pp. 2670–2675.